JOURNAL OF AIRCRAFT
Vol. 48, No. 2, March–April 2011

Modeling of Flight Dynamics of Morphing-Wing Aircraft

B. Obradovic* and K. Subbarao†
University of Texas at Arlington, Arlington, Texas 76019

DOI: 10.2514/1.C000269

Aircraft with variable wing geometry (morphable wings) are of considerable interest, not only for mission-specific optimization but for enhanced maneuverability as well. In the nascent field of mini or micro unmanned aerial vehicles, large and rapid changes in wing geometry are achievable, resulting in significant changes of the dynamics of the vehicle. In this paper, a simulation methodology suitable for such aircraft is presented, accounting for the changes in both the aerodynamic and inertial properties. Because of the complexity of the possible wing configurations, the aerodynamics are simulated using an unsteady vortex-lattice approach, solved concurrently with six-degree-of-freedom (+) nonlinear equations of motion. The time dependence of the inertia tensor and motion of mass within the body frame are explicitly taken into account, resulting in additional body-frame forces and moments. The simulation methodology is applied to various gull-wing configurations, and the flight dynamics are analyzed through nonlinear simulation.

Nomenclature

$\mathbf{F}$	=	net force acting on aircraft
$\mathbf{F_j}$	=	jth morphing force ($j \in \{1, 4\}$)
$[\mathbf{H_i}]$	=	Hessian matrix of ith panel center with regard to morphing variables
$[\boldsymbol{J}]$	=	moment of inertia tensor
m	=	mass of aircraft
$\mathbf{M}_j$	=	jth morphing moment ($j \in \{1, 4\}$)
$\hat{\mathbf{n}}_i$	=	normal vector of ith panel
$\mathbf{r}$	=	position of a mass element within the body frame
$\tilde{\boldsymbol{r}}$	=	skew-symmetric matrix representation of r
$\mathbf{R_{cm}}$	=	position of aircraft center of mass with regard to inertial frame
$\mathbf{R_f}$	=	position of body-frame origin with regard to inertial frame
$\mathbf{r_{cm}}$	=	position of aircraft center of mass within body frame
$\mathbf{V_f}$	=	velocity of origin of aircraft body frame
$\mathbf{v}'$	=	velocity of a mass element in the body frame (body-frame derivative of r)
$\mathbf{x}_i$	=	position of center of ith aircraft panel in body frame
Γ_i	=	induced vorticity of ith vortex-lattice element
$\boldsymbol{\Delta r}_{\mathrm{cm}}$	=	displacement of aircraft center of mass from body-frame origin
ρ	=	mass density (of air or aircraft, depending on context)
$\boldsymbol{\tau_{ext}}$	=	total external moment acting on aircraft
Φ	=	total airflow velocity potential
Φ_∞	=	freestream velocity potential
ϕ_i	=	velocity potential induced by ith panel
$\boldsymbol{\omega}$	=	angular velocity of body frame with regard to the inertial frame
$[\tilde{\boldsymbol{\omega}}]$	=	skew-symmetric matrix representation of $\boldsymbol{\omega}$

Presented as Paper 2009-6240 at the AIAA Modeling and Simulation Technologies Conference, Chicago, IL, 10–13 August 2009; received 22 January 2010; revision received 24 November 2010; accepted for publication 5 December 2010.

*Department of Mechanical and Aerospace Engineering; borna.obradovic@gmail.com. Student Member AIAA.

†Associate Professor, Department of Mechanical and Aerospace Engineering; subbarao@uta.edu. Life Member AIAA.

I. Introduction

VARIABLE-WING geometry aircraft have been in regular use since the 1970s, and examples of attempts at morphable wings date back to the pre-World War II era [1]. The goal of wing morphing was primarily mission-specific optimization of aerodynamic performance. Thus, swing wings were used to provide high lift-to-drag ratio (L/D) in the unswept position for low-speed takeoff and landing and reduced drag at high speed cruise in the sweptback position. More recently, there has been considerable interest in the use of rapidly morphing wings for the purpose of enhanced maneuverability. This implies rapid motion of large sections of the wing. While this may be difficult to achieve for a large aircraft, it is quite feasible for mini or micro unmanned aerial vehicles (UAVs). Greatly enhanced maneuverability has been demonstrated for morphable-wing UAVs [2,3], and roll rates in excess of 360 deg/s have been achieved [2]. Furthermore, research is being conducted into the utility of biomimetic flight for micro UAVs [4], requiring significant and rapid wing morphing.

The subjects of dynamics and control of morphing aircraft have received considerable attention in the literature. This is particularly true in the last several years, as the notion of morphing has been applied to UAVs. The effect of morphing on the dynamics is studied in [5–8]. Simplified flight dynamics are used, ignoring terms deemed to be insignificant. It is shown in this work, however, that the additional terms are quite significant if the morphing involves a large amplitude or a high morphing rate. The additional terms introduced in the literature are typically just the time derivatives of the inertia tensor components. In [6,8], the morphing inputs are assumed to directly modify the inertia tensor. Linearization of the dynamics then results in a linear time-varying system, the stability properties of which are further examined in [5]. A more complete dynamical model is formulated in [9]; the equations of motion (EOMs) are rederived with the assumption of morphing, resulting in additional terms (beyond the time derivatives of the inertia tensor). However, the development is restricted to symmetric and/or purely longitudinal morphing, which allows the authors to omit otherwise significant coupling terms. A subset of morphing strategies confined (primarily) to airfoil shape is also studied in [10]. The morphing flight dynamics are limited to the time derivatives of the inertia tensor. The dynamics of morphing are also studied in the context of multibody dynamics [11]. Using the constrained-dynamics software ADAMS [12] for solving the multibody dynamics problem using the augmented formulation [13], a rigorous simulation of symmetric (and slow) gull-wing morphing is obtained. While accurate, the multibody approach does not result in particularly insightful analytic expressions describing morphing.

The subjects of aerodynamics and airflow for morphing aircraft have also been studied by several groups. Various panel approaches

have been used [10,14,15], demonstrating the applicability of the method. Also shown [14] is that there is relatively little improvement in accuracy to be had by using fully unsteady lattice methods (as opposed to using a quasi-stationary vortex lattice or doublet lattice), except for in special circumstances (such as helicopter rotors or near-hover flight). An unsteady model of the wake is not needed for this work, due to the low ratio of the morphing to forward aircraft velocities. Any disturbances introduced into the wake by morphing quickly fall away from the aircraft and have little influence on aerodynamics. The quasi-static wake is therefore a reasonable approximation, as long as the morphing velocity (i.e., motion of wing panels) is slow compared with the forward velocity of the aircraft, as is considered in this work. Lattice methods are shown to be significantly more predictive than lifting-line theory, however. This has important implications on the choice of method when attempting to balance accuracy and computational efficiency. Efforts to leverage full Navier–Stokes computational fluid dynamics (CFD) for morphing aircraft simulation are more limited, due to the obvious computational effort involved. Nevertheless, the unsteady aerodynamics of morphing are studied in [16].

From theoretical and computational analysis standpoints, large and rapid changes of the wing geometry present some unique challenges. First, the number of degrees of freedom (DOFs) that strongly influence the aerodynamics is increased, possibly greatly, depending on the complexity of the wing. This in turn implies that precomputing aerodynamic derivatives becomes combinatorially prohibitive; the dimensionality of the configuration space is potentially very high, and interactions cannot be a priori neglected due to large deflections. The full lookup table of derivatives would have to be recomputed for any change in the aircraft structure. This suggests that computing the aerodynamic forces during the flight simulation may be preferable.

Second, the large motions of the wing segments make the rigid-body approximation of the aircraft inadequate. In a frame fixed to a predetermined point on the aircraft, both the inertia tensor and center of mass (CM) are functions of time. This must be taken into account in the EOMs. Alternatively, the aircraft can be treated as a multibody system, with each movable segment being represented by a rigid body [13,17]. Such approaches, while more detailed, add significant computational cost and complexity.

Lastly, since high maneuverability is the goal, unsteady aerodynamic effects must also be addressed. Specifically, the within-body-frame motion of the wings, as well as the rotational velocity of the body frame itself, must be modeled [18].

In this paper, a simulation methodology well suited to handle the aforementioned challenges is presented. A general-purpose unsteady vortex-lattice aerodynamics simulator is developed and coupled to the transient simulation of a six-DOF (+) aircraft. Simulations are then performed with several different morphable-wing aircraft configurations, and results are analyzed. The approach used results in considerably less computational effort than the standard flavors of multibody dynamics, but it is nevertheless suitable for all simulations in which the structural dynamics do not play a critical role.

The simulation software supports several types of computations: wind-tunnel aerodynamic simulation, trim solution, stability matrix computation (linearization), and fully nonlinear transient simulation. The simulation infrastructure is set up as a MATLAB class library with two basic types: models and solvers. Various models can be attached to different solvers, since a common interface is used by all. The key model components are the aerodynamics, flight dynamics, and morphing. Potentially, the most computationally demanding element is the aerodynamic calculation using the vortex-lattice model (VLM). It is therefore implemented as a C++ class library, interfaced to MATLAB using a MEX function or accessed through a programmable tool command language/toolkit (TCL/TK) [19] interface. The infrastructure is illustrated in Fig. 1.

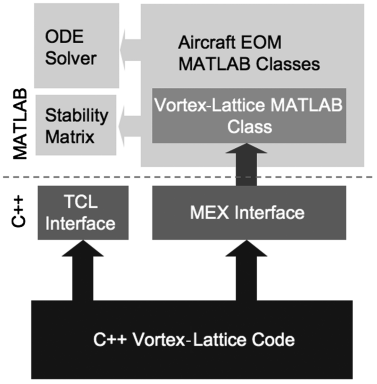

Fig. 1 Overview of software infrastructure for morphing-wing code.

II. Modeling of Aerodynamics

The use of a VLM at each time step eliminates the combinatorial increase in the lookup-table size for complex aircraft. Thus, while the complexity and time for a single simulation are inevitably increased, the overall analysis and design time are arguably decreased. Additionally, questions about the truncation errors induced by interpolation, or even extrapolation, from sparse multidimensional tables are removed. Numerous vortex-lattice schemes have been studied and used [15,18], with varying tradeoffs of detail and complexity.

In this work, the no-penetration condition of the potential flow problem is solved using horseshoe vortex elements with a freestream-aligned trailing vortex. The system of equations of the VLM to be solved is given by Eq. (1):

$$\sum_j (\hat{\mathbf{n}}_i \cdot \nabla\phi_j)\Gamma_j = -\hat{\mathbf{n}}_i \cdot (\nabla\Phi_\infty + [\boldsymbol{\omega}]\boldsymbol{r}_i + \mathbf{v}_i) \tag{1}$$

In Eq. (1), ϕ_j represents the velocity potential induced by the jth vortex, Φ_∞ is the freestream velocity potential, $\boldsymbol{\omega}$ represents the angular velocity of the body frame, $\boldsymbol{r}_i$ is the position vector of the ith control point, and $\mathbf{v}_i$ is the body-frame velocity of the control point, which is due to the morphing of the wings. The unit vector $\hat{\mathbf{n}}_i$ represents the normal of each panel. The mean-camber shape of each planform is user specified, and the normal vector for each panel of the discretization is computed accordingly. The mean-camber profile can vary in the span direction, although a constant profile is used in this work. Thus, even though the thickness of the panels is neglected, the mean shape is taken into account. This is particularly important for obtaining the correct 0° angle of attack, lift, and induced drag, in general.

As is standard for vortex-lattice methods, the velocity potential is obtained by the superposition of contributions of all the vortex elements using the Biot–Savart law [18]. The strength of each vortex represents the solution of the linear system of equations formed by applying Eq. (1) to each control point. Therefore, the VLM considered a lifting surface interference method.

The angular velocity and morphing velocity terms are included, since they present significant contributions to aerodynamic damping, and the velocity of the morphing-wing panels may be comparable with (or greater than) the velocity of the body-frame rotational motion. The additional terms effectively represent a local freestream velocity, which ultimately manifests as a damping term in the EOMs. In the special case of the rigid aircraft, the last term vanishes. Neglecting the angular velocity term leads to the standard quasi-stationary vortex-lattice method [15,18,20]. However, doing so eliminates the damping terms, which must then be added analytically. In this work, all terms in Eq. (1) are retained, at essentially no computational cost. The influence of the rotational terms is strongest at low freestream velocity; thus, it is most relevant for a low-speed highly maneuverable UAV.

It must be noted here that the vortex wake is not treated in unsteady fashion. Thus, the method used is not a full unsteady VLM. Studies [14] have shown that, for most situations, the time dependence of the vortex wake has only a small influence on aircraft dynamics, with the exception of special cases, such as helicopter rotors, and near-hover and flapping flight. As previously discussed, the forward velocity of the aircraft is assumed to be much higher than the morphing velocity,

making the vortex wake essentially quasi static. The additional (significant) computational expense of the unsteady vortex wake is thus not included.

Forces and moments on the panels, planforms, and complete aircraft are computed by a summation of the individual forces across all the panels. Thus, we have

$$\mathbf{F} = \sum_i \rho[\tilde{\mathbf{V}}_\mathbf{i}]\Gamma_i \tag{2}$$

$$\boldsymbol{\tau}_{\mathbf{area}} = \sum_i \rho[\tilde{\mathbf{r}}_i]([\tilde{\mathbf{V}}_\mathbf{i}]\Gamma_i) \tag{3}$$

where $\mathbf{r}_i$ is the position vector of the ith panel (relative to the origin of the body coordinate system), and $\mathbf{V}_i$ is the local airstream velocity at the ith control point. The direct method used here requires more computation than methods based on vorticity or flowfield alone, but it provides more detailed information about the distribution of the aerodynamic loads and three-dimensional forces and moments.

The vortex distribution is discretized on a nonuniform tensor mesh, with a mesh assigned to each planform (or volume, with ring vortices only in this case). The use of the nonuniform mesh is essential for reducing the number of elements required for a converged solution. This is particularly true for the induced drag, which is very sensitive to the vorticity distribution near the leading edge of a wing. The nonuniform meshing algorithm begins by partitioning polygonal planforms into trapezoids. The spanwise direction of the mesh is uniform, whereas the chordwise direction is highly nonuniform. The trailing half of the wing, where the vorticity is expected to be weak and slowly varying, has a uniform and sparse mesh. A geometrically contracting mesh with a constant ratio is used in the leading half of the planform. The smallest and largest mesh spacings are user defined.

III. Modeling of Flight Dynamics

Given that significant changes of the aircraft geometry take place, it is clear that the standard rigid-body EOMs will not be applicable. Several approaches could be used to remedy the situation. One possibility is to apply the methods of multibody dynamics [13,17], treating each moving part of the aircraft as a separate rigid body. Depending on the choice of submethod, this results in either a large system of loosely coupled ordinary differential equations (ODEs) and a set of algebraic constraint equations [13] or a tightly coupled, highly nonlinear set of ODEs [17]. Either possibility entails a significantly greater computational effort than rigid-body dynamics.

Another approach is to continue to treat the morphing aircraft as a single body but relax the condition of rigidity. Thus, the inertia tensor becomes an explicit function of time, since it depends on the displacements and rotations of the various components of the aircraft. Additionally, the CM of the aircraft will generally not be fixed in the body frame. The aircraft is placed into the body frame such that the CM of the unmorphed aircraft is at the origin. As the aircraft morphs, however, the instantaneous CM will not generally coincide with the body-frame origin. This is expected to result in a modification of the EOMs, since they are usually written with the assumption of coincident CM and body-frame origin. In spite of this complication, the computational effort is considerably smaller than with either flavor of multibody dynamics, as will be demonstrated. Therefore, relaxing the rigidity is the method of choice in this work. It must be pointed out, however, that by making the aircraft configuration an explicit function of time, we have neglected the detailed actuator dynamics as well as the constraint and actuator forces and moments required to produce the desired aircraft configuration. We simply assume that the aircraft is able to achieve the desired configuration, If needed, the actual magnitudes of the moments and required power can be postprocessed.

A time-stepping ODE integration scheme is used to propagate the EOMs of the six-DOF (+) aircraft, while the aerodynamic forces are evaluated at each time step using an unsteady VLM [18]. The overall simulation flow is illustrated in Fig. 2.

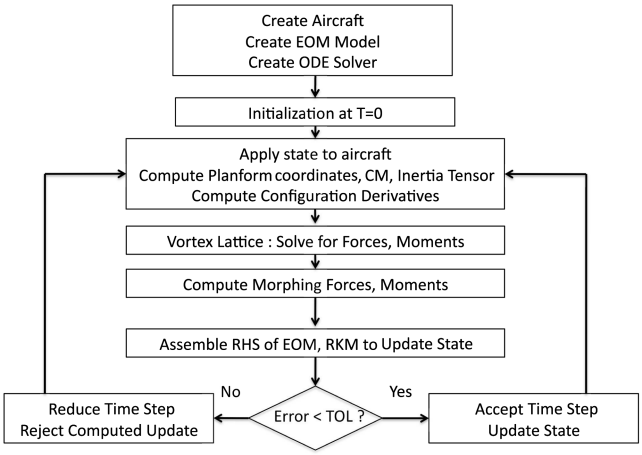

Fig. 2 Simulation flow with error estimation and adaptive time stepping. (RKM denotes Runge–Kutta–Merson, and TOL denotes tolerance.)

Once the aircraft geometry has been defined in terms of a set of planforms, as described by the first step in Fig. 2, the actual time-stepping simulation can begin. The key steps are the computation of geometry, based on the current morphing variables, the solution of the VLM and the aerodynamic forces, the computation of morphing forces and moments, and finally the update of the aircraft state based on the EOMs.

A. Rotational Equations of Motion

To derive the appropriate EOMs, we start with rotational dynamics in the inertial frame, using the flat-Earth assumption. The angular momentum is obtained from [21]:

$$\boldsymbol{\tau}_{\mathbf{ext}} = \dot{\mathbf{h}} + m\Delta\tilde{\mathbf{r}}_{\mathbf{cm}}\dot{\mathbf{V}}_\mathbf{f} \tag{4}$$

In Eq. (4), $\boldsymbol{\tau}_{\mathbf{ext}}$ denotes the total applied moment (from aerodynamic, propulsive, and gravitational forces), m is the total mass of the aircraft, $\boldsymbol{\Delta}\tilde{\boldsymbol{r}}_{\mathbf{cm}}$ is the displacement of the CM from the origin of the body frame (in skew-symmetric matrix form), and $\dot{\mathbf{V}}_\mathbf{f}$ is the inertial-frame velocity of the body-frame origin. The derivatives in Eq. (4) are all expressed in the inertial frame. The angular momentum in the body frame can be expressed as

$$\mathbf{h} = \int \tilde{\mathbf{r}}([\tilde{\boldsymbol{\omega}}]\mathbf{r} + \mathbf{v}')\,\mathrm{d}m = [\mathbf{J}]\omega + \int \tilde{\mathbf{r}}\mathbf{v}'\,\mathrm{d}m \tag{5}$$

The integration is taken over the entire mass of the aircraft. The term $[\tilde{\mathbf{r}}]$ is the skew-symmetric representation of the position of the mass element dm, $[\tilde{\boldsymbol{\omega}}]$ is the skew-symmetric representation of the body-frame angular velocity, and $\mathbf{v}'$ is the body-frame morphing-induced velocity of the mass element dm. The final velocity term is unique to the morphing aircraft, and it results in the integral on the right-hand side (RHS) of Eq. (5). The term $[\mathbf{J}]\boldsymbol{\omega}$ is simply the standard expression for the angular momentum of a rigid body. The rate of change of the body-frame angular momentum can then be expressed as

$$[\mathbf{J}]\dot{\boldsymbol{\omega}} + [\dot{\mathbf{J}}]\boldsymbol{\omega} + \int([\tilde{\dot{\mathbf{r}}}]\mathbf{v}' + [\tilde{\mathbf{r}}]\dot{\mathbf{v}}')\,\mathrm{d}m + [\tilde{\boldsymbol{\omega}}][\mathbf{J}]\boldsymbol{\omega} + [\tilde{\boldsymbol{\omega}}]\int[\tilde{\mathbf{r}}]\mathbf{v}'\,\mathrm{d}m$$
$$= \boldsymbol{\tau}_{\mathbf{ext}} - m\Delta[\tilde{\mathbf{r}}_{\mathbf{cm}}](\dot{\mathbf{V}}_\mathbf{f} + [\tilde{\boldsymbol{\omega}}]\mathbf{V}_\mathbf{f}) \tag{6}$$

The derivatives in Eq. (6) are expressed in the body frame. The first term in the leftmost integral vanishes, and we are left we the rotational equation of motion of the morphing aircraft in the body frame:

$$[\mathbf{J}]\dot{\boldsymbol{\omega}} = \boldsymbol{\tau}_{\mathbf{ext}} - [\tilde{\boldsymbol{\omega}}][\mathbf{J}]\boldsymbol{\omega} - \left([\dot{\mathbf{J}}]\boldsymbol{\omega} + m[\Delta\tilde{\mathbf{r}}_{\mathbf{cm}}](\dot{\mathbf{V}}_{\mathbf{f}} + [\tilde{\boldsymbol{\omega}}]\mathbf{V}_{\mathbf{f}}) + [\tilde{\boldsymbol{\omega}}]\int[\tilde{\mathbf{r}}]\mathbf{v}'\,\mathrm{d}m + \int[\tilde{\mathbf{r}}]\dot{\mathbf{v}}'\,\mathrm{d}m\right) \tag{7}$$

The terms in parentheses on the RHS of Eq. (7) are moments that are not present in the standard Euler equations for rigid-body motion. They are referred to as morphing moments in this work. Explicitly, they arise from the displacement of the CM from the body-frame origin, the rate of change of the inertia tensor, and the body-frame motion of mass within the aircraft. For the sake of notational compactness in subsequent sections, the morphing moments will be labeled as follows:

$$\mathbf{M}_{\mathbf{1}} = -[\dot{\mathbf{J}}]\boldsymbol{\omega} \tag{8}$$

$$\mathbf{M}_{\mathbf{2}} = -m[\Delta\tilde{\mathbf{r}}_{\mathbf{cm}}]\cdot(\dot{\mathbf{V}}_{\mathbf{f}} + [\tilde{\boldsymbol{\omega}}]\mathbf{V}_{\mathbf{f}}) \tag{9}$$

$$\mathbf{M}_{\mathbf{3}} = -[\tilde{\boldsymbol{\omega}}]\int[\tilde{\mathbf{r}}]\mathbf{v}'\,\mathrm{d}m \tag{10}$$

$$\mathbf{M}_{\mathbf{4}} = -\int[\tilde{\mathbf{r}}]\dot{\mathbf{v}}'\,\mathrm{d}m \tag{11}$$

For the special case of the rigid body, the morphing moments vanish, the inertia tensor is constant, and the rotational dynamics revert to the Euler equations. The final two terms involve nontrivial integrals and must be treated numerically (described in subsequent section). The relative importance of the various morphing moments will naturally depend on the aircraft, as well as the flight conditions. This is studied in more detail on several morphing-induced turns in Secs. IV.A and IV.B.

B. Translational Equations of Motion

The translational dynamics are handled similarly to the rotational dynamics. The CM is not fixed at the body-frame origin. The position, velocity, and acceleration of the CM in the inertial frame can then be written as

$$\mathbf{R}_{\mathbf{cm}} = \mathbf{R}_{\mathbf{f}} + \boldsymbol{\Delta}\mathbf{r}_{\mathbf{cm}} \tag{12}$$

$$\mathbf{V}_{\mathbf{cm}} = \mathbf{V}_{\mathbf{f}} + \boldsymbol{\Delta}\dot{\mathbf{r}}_{\mathbf{cm}} + [\tilde{\boldsymbol{\omega}}]\mathbf{r}_{\mathbf{cm}} \tag{13}$$

$$\dot{\mathbf{V}}_{\mathbf{cm}} = \dot{\mathbf{V}}_{\mathbf{f}} + [\tilde{\boldsymbol{\omega}}]\mathbf{V}_{\mathbf{f}} + \boldsymbol{\Delta}\ddot{\mathbf{r}}_{\mathbf{cm}} + 2[\tilde{\boldsymbol{\omega}}]\dot{\mathbf{r}}_{\mathbf{cm}} + [\dot{\tilde{\boldsymbol{\omega}}}]\boldsymbol{\Delta}\mathbf{r}_{\mathbf{cm}} + [\tilde{\boldsymbol{\omega}}][\tilde{\boldsymbol{\omega}}]\boldsymbol{\Delta}\mathbf{r}_{\mathbf{cm}} \tag{14}$$

The equation of motion of the CM is simply given as

$$\dot{\mathbf{V}}_{\mathbf{cm}} = \frac{\mathbf{F}_{\mathbf{ext}}}{m} + \mathbf{g} \tag{15}$$

where $\mathbf{F}_{\mathbf{ext}}$ represents the aerodynamic and propulsive forces acting on the aircraft. Inserting Eq. (14) into Eq. (15), the equation of motion for the origin of the body frame is obtained:

$$m\dot{\mathbf{V}}_{\mathbf{f}} = \mathbf{F}_{\mathbf{ext}} + m\mathbf{g} - m[\tilde{\boldsymbol{\omega}}]\mathbf{V}_{\mathbf{f}} - (m\boldsymbol{\Delta}\ddot{\mathbf{r}}_{\mathbf{cm}} + 2m[\tilde{\boldsymbol{\omega}}]\dot{\mathbf{r}}_{\mathbf{cm}} + m[\dot{\tilde{\boldsymbol{\omega}}}]\boldsymbol{\Delta}\mathbf{r}_{\mathbf{cm}} + m[\tilde{\boldsymbol{\omega}}][\tilde{\boldsymbol{\omega}}]\boldsymbol{\Delta}\mathbf{r}_{\mathbf{cm}}) \tag{16}$$

As was the case with rotational dynamics, the translational dynamics exhibit additional terms [in parentheses in Eq. (16)] as compared with the standard rigid-body equations. The additional terms depend on the displacement of the CM (relative to the origin of the body frame), as well as its first and second derivatives. As in the case of the morphing moments, we define the morphing forces as

$$\mathbf{F}_{\mathbf{1}} = -m\boldsymbol{\Delta}\ddot{\mathbf{r}}_{\mathbf{cm}} \tag{17}$$

$$\mathbf{F}_{\mathbf{2}} = -2m[\tilde{\boldsymbol{\omega}}]\boldsymbol{\Delta}\dot{\mathbf{r}}_{\mathbf{cm}} \tag{18}$$

$$\mathbf{F}_{\mathbf{3}} = -m[\dot{\tilde{\boldsymbol{\omega}}}]\boldsymbol{\Delta}\mathbf{r}_{\mathbf{cm}} \tag{19}$$

$$\mathbf{F}_{\mathbf{4}} = -m[\tilde{\boldsymbol{\omega}}][\tilde{\boldsymbol{\omega}}]\boldsymbol{\Delta}\mathbf{r}_{\mathbf{cm}} \tag{20}$$

C. Modeling of Morphing

Since the aircraft undergoes morphing, various dynamic properties must change in the body frame. For example, the $\boldsymbol{\Delta}\mathbf{r}_{\mathbf{cm}}$ term is a function of the applied configuration q; rotations and displacements $\{q_1, q_2, \ldots, q_n\}$ of wing sections (or other parts of the aircraft) result in changes of $\boldsymbol{\Delta}\mathbf{r}_{\mathbf{cm}}$, and the same is true for the inertia tensor. In reality, however, these deflections cannot occur instantaneously. Had a multibody dynamics approach been used instead, this would have arisen naturally. In the present formulation, however, the dynamics of the actuation have to be introduced separately. In addition, a model for the dynamics must be used, since the deflections are not handled explicitly. Additional state variables are introduced for the displacements $\{q_1, q_2, \ldots, q_n\}$. Since the equations of translational dynamics involve the second derivative of the CM displacement (itself a function of the configuration variables), a second-order system is needed to describe the dynamics of each configuration variable. Thus, we also define the state variables $\{p_1, p_2, \ldots, p_n\}$, with $p_i = \dot{q}_i$. The desired or control input set is then $\{q_{c1}, q_{c2}, \ldots, q_{cn}\}$. A suitable second-order system is simply

$$\dot{p}_i = -2\xi_i\omega_i p_i - \omega_i^2(q_i - q_{ci}) \tag{21}$$

$$\dot{q}_i = p_i \tag{22}$$

with the parameters ω and ξ suitably chosen to model each actuator. It is noted that this approach ignores the effect of loading on the actuator dynamics. Implicitly, the actuators themselves are assumed to be controlled by a model-following control system and can provide the required moments and power to assert behavior, as described by Eqs. (21) and (22). If this is not the case for a given system of interest, it should be modeled using multibody dynamics instead.

Once the dynamics of the actuators have been defined, the instantaneous positions of the planforms, the CM, and the instantaneous inertia tensor, as well as the derivatives of all the body-frame quantities, can all be computed. The panel coordinates are updated by recursive rotation, as dictated by the updated morphing states. Once the panel coordinates and orientations are known, the instantaneous coordinates of the CM are simply obtained as

$$\mathbf{r}_{\mathbf{cm}} = \frac{1}{m}\sum_i \mathbf{r}_{\mathbf{i}} m_i \tag{23}$$

where $\mathbf{r}_{\mathbf{i}}$ is the position of the CM of the ith planform of which the aircraft is comprised (including the fuselage). The position of the CM of each planform is updated as the panel is rotated, translated, or stretched. Likewise, the instantaneous moment of inertia tensor is computed as

$$[\mathbf{J}'] = \sum_i [[\mathbf{R}_{\mathbf{i}}]^{\mathbf{T}}[\mathbf{J}_{\mathbf{i}}][\mathbf{R}_{\mathbf{i}}] + m_i[\boldsymbol{\Delta}\tilde{\mathbf{r}}_{\mathbf{i}}][\boldsymbol{\Delta}\tilde{\mathbf{r}}_{\mathbf{i}}]^{\mathbf{T}}] \tag{24}$$

where $[\mathbf{J}']$ is the instantaneous moment of inertia in the body frame, $[\mathbf{J}_{\mathbf{i}}]$ is the moment of inertia of the ith planform in the reference position (before rotation or translation), m_i is the mass of the ith planform, $[\mathbf{R}_{\mathbf{i}}]$ is the rotation matrix of the ith planform relative to the inertial frame, and $\boldsymbol{\Delta}\tilde{\mathbf{r}}_{\mathbf{i}}$ is the position of the CM of the ith planform.

The EOMs require the computation of the first and second derivatives of the CM as well as the first derivative of the inertia

tensor. Since the aircraft can be arbitrarily complex, an analytical solution is not practical. Instead, the derivatives are computed numerically. However, it is important to avoid using finite differencing in time to obtain the derivatives. This would introduce a time-step-dependent truncation error into the expression for the time derivative of the configuration variables. Doing so would necessarily increase the truncation error of the ODE step. Instead, the derivatives are computed as follows (where x_i represents a panel position vector or the CM vector):

$$\mathbf{x}_\mathbf{i} = \mathbf{x}_\mathbf{i}(q_1, q_2, \ldots, q_n) \tag{25}$$

$$\dot{\mathbf{x}}_\mathbf{i} = \sum_k \frac{\partial \mathbf{x}_\mathbf{i}}{\partial q_k}\dot{q}_k \tag{26}$$

$$\ddot{\mathbf{x}}_\mathbf{i} = \dot{\mathbf{q}}^\mathbf{T}[\mathbf{H}_\mathbf{i}]\dot{\mathbf{q}} + \sum_k \frac{\partial \mathbf{x}_\mathbf{i}}{\partial q_k}\ddot{q}_k \tag{27}$$

where the Hessian term $[\mathbf{H}_\mathbf{i}]$ is defined as

$$[\mathbf{H}_\mathbf{i}]_\mathbf{jk} = \frac{\partial^2 \mathbf{x}_\mathbf{i}}{\partial q_j \partial q_k} \tag{28}$$

Note that each element of the matrix $[\mathbf{H}_\mathbf{i}]$ in Eqs. (28) and (29) is a three-dimensional vector. Similarly, the time derivatives of the inertia tensor can be expressed as

$$\frac{\mathrm{d}[\mathbf{J}]}{\mathrm{d}t} = \sum_n \frac{\partial[\mathbf{J}]}{\partial q_n}\dot{q}_n \tag{29}$$

The temporal derivatives of the panel coordinates, the planform, and the aircraft CM, as well as the inertia tensor components, are computed using numerical differentiation with regard to actuator positional variables only. The Jacobian for the mapping between the configuration-space variables (panel and CM coordinates and velocities) and the morphing variables is computed numerically. Time derivatives are included implicitly in the state variables $\dot{q}_i$. Since the accuracy of the numerical derivatives with regard to the actuator kinematic variables is independent of the local ODE integration time step Δt, the order of the local truncation error with regard to Δt does not change. The actual computation of the Jacobians with regard to the actuator positions is carried out by performing a set of virtual displacements of the actuator positions at every time step and using central differences to compute the derivative values. Only a minimal computational overhead is incurred. Numerical integration is required for the final two morphing moments. These are

$$\mathbf{M}_\mathbf{3} = [\tilde{\boldsymbol{\omega}}]\int [\tilde{\mathbf{r}}]\mathbf{v}'\,\mathrm{d}m \approx [\tilde{\boldsymbol{\omega}}]\sum_i [\tilde{\mathbf{r}}]_\mathbf{i}\mathbf{v}'_\mathbf{i}m_i \tag{30}$$

and

$$\mathbf{M}_\mathbf{4} = \int [\tilde{\mathbf{r}}]\dot{\mathbf{v}}'\,\mathrm{d}m \approx \sum [\tilde{\mathbf{r}}_\mathbf{i}]\dot{\mathbf{v}}'_i m_i \tag{31}$$

The terms inside the integrals are the positions and velocities of the mass elements of the aircraft. Since there is no closed-form solution to the integrals for M_3 and M_4 for an arbitrary aircraft, the values of M_3 and M_4 are obtained numerically at each time step. A natural discretization of the moving planforms is already available for the vortex-lattice mesh.

However, this potentially represents a large number of points for velocity and acceleration calculations, so the vortex-lattice panels are grouped into a smaller number of larger, nontrapezoidal panels. The positions, velocities, and accelerations of the CM of these shapes is then used for the computation of M_3 and M_4. Testing indicates that the values of M_3 and M_4 are converged with as few as six to eight panels per planform. The velocities and accelerations are computed based on the positions, using Eqs. (26) and (27).

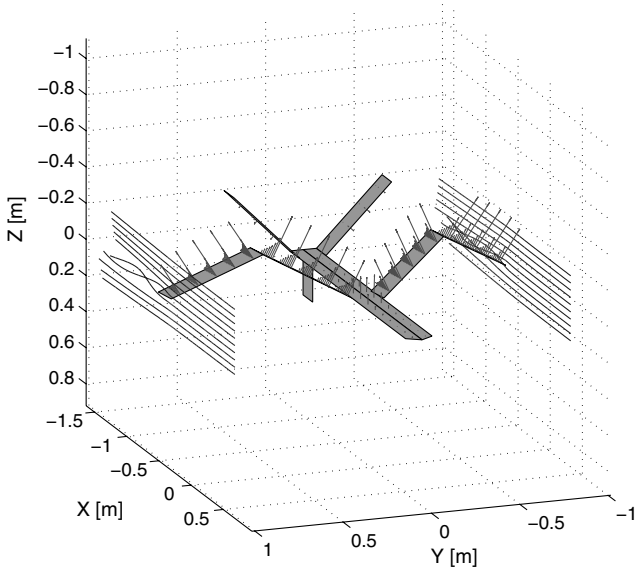

Fig. 3 The reference symmetric gull-wing configuration, with airflow streamlines and aerodynamic forces.

IV. Application to Morphable-Wing Configurations

To test the utility of the simulation methodology, it is applied to several morphable-wing configurations. The test aircraft of choice is a gull-wing-type aircraft, illustrated in its reference configuration in Fig. 3. The basic properties of the aircraft are summarized in Table 1. The conventional aileron and flap control surfaces have been replaced by movable wing sections, which take on the roles of the ailerons and flaps. Twin conventional ruddervons (combined twin rudder and elevons) are placed in the back of the aircraft and provide pitch and yaw control. The aircraft is a small UAV operating in the high-Re incompressible regime, with a freestream Mach number less than 0.3.

For each configuration, the aerodynamic impact of the wing morphing is first evaluated in a wind-tunnel simulation, followed by a flight simulation which uses the full, nonlinear dynamics. The emphasis is on understanding the dynamics of maneuvering using morphing rather than quasi-static performance. Thus, the behavior of a morphing-wing aircraft while performing a rapid turn is examined. The turning moments are provided exclusively by wing morphing.

A. Asymmetric Gull Wing

1. Static Analysis

It is evident from the forces illustrated in Fig. 4 that the asymmetry in the aerodynamic forces will result in a roll moment, as shown in Fig. 5. In Fig. 5, the wing is deflected from the configuration shown in Fig. 3, a trim point for the aircraft. The roll moment is simply due to the reduction of the vertical component of the aerodynamic forces on the gull wing, which is not present in the flat wing. In addition to the roll moment, Fig. 5 also indicates the presence of a yaw moment. The yaw moment arises due to a combination of morphing and wing sweep. The right wing, which remains V shaped, has Y-directed force

Table 1 Gull-wing aircraft basic properties

Parameter	Value
Length	2 m
Wingspan	2 m
Area	0.87 m^2
Mass	50 kg
I_{xx}	10 kg m^2
I_{yy}	17 kg m^2
I_{zz}	11 kg m^2
I_{xz}	−1.8 kg m^2
Mach number (cruise)	0.2–0.25

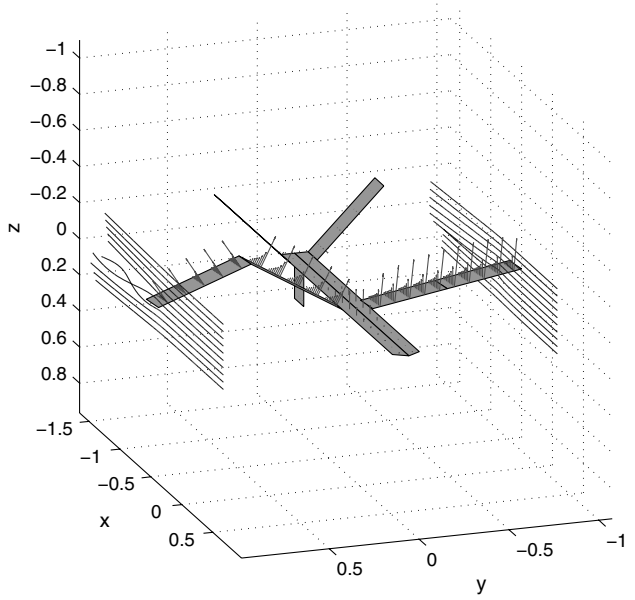

Fig. 4 The asymmetric gull-wing configuration, with airflow streamlines and aerodynamic forces.

components, as can be seen from Fig. 4. The two portions of the wing thus contribute oppositely directed yaw moments around the CM, but the outer wing has a larger moment arm (due to wing sweep), and the overall yawing moment is therefore negative. The yawing moment tends to turn the aircraft counter to the induced roll, which creates a positive slip angle. Thus, without ruddervon (combined twin rudder and elevons) inputs, the initial yaw motion of the aircraft is expected to be nose left, while the roll is to the right. As the slip angle β becomes positive, however, a stabilizing yawing moment from the ruddervons and the vertical tail are expected to keep the sideslip angle in check. Finally, the increased lift of the left wing also leads to positive pitching moment, since the ruddervons were trimmed to compensate for the lift of the symmetric gull wing. Thus, an initial pitch-up tendency is expected as well.

2. *Flight Simulation*

Having established the expectations for the aerodynamic forces on the asymmetric gull wing in the previous section, the full, nonlinear flight simulation of a morphing-induced turn is examined next. The starting configuration in this maneuver is the symmetric gull wing, shown in Fig. 3. The gull-wing angle, ruddervon angle, and thrust are trimmed to provide level flight at 90 m/s. At this airspeed, the wings provide sufficient lift at a gull-wing angle of $\approx 30°$. At $t = 15$ s, the

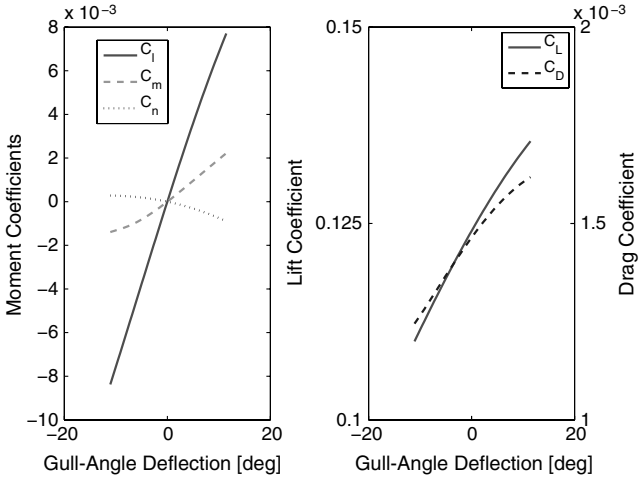

Fig. 5 The behavior of lift and moments as a function of the gull-angle deflection.

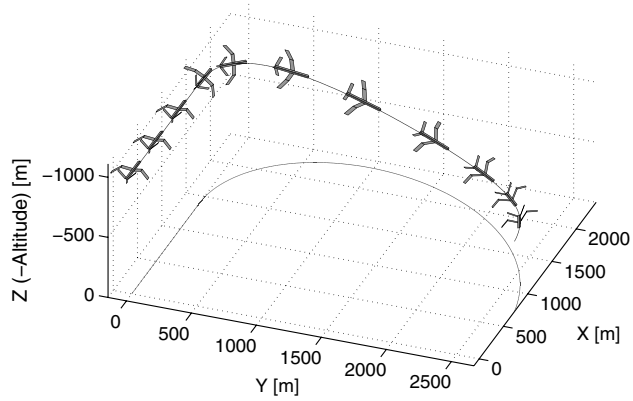

Fig. 6 The turning trajectory induced by asymmetric wing morphing.

turn maneuver is initiated by flattening the left wing; the left gull-wing angle is reduced to 0°. The resulting trajectory is illustrated in Fig. 6. The time dependence of the wing angles is shown in Fig. 7. The resulting body-frame motion of the CM is illustrated in Fig. 8. The time dependence of the inertia tensor is shown in Fig. 9. As discussed in the previous section, rolling, yawing, and pitching aerodynamic moments are all induced by this maneuver. Additionally, morphing moments M_1 through M_4 must be considered in the analysis.

The overall behavior of the aircraft during the turn is illustrated in Figs. 6–11. The angular velocity exhibits the expected spike in roll, induced largely by aerodynamic moments. Additionally, α and β both increase, as expected, due to the aerodynamic pitch and yaw moments. However, the fine detail of the motion hints at additional contributions. Indeed, the morphing moments for this configuration are nonnegligible, as evidenced in Fig. 10. While the pitch and yaw moments are dominated by the aerodynamic contributions, a significant contribution to the roll moment comes from the morphing moments themselves. It can be seen that the M_4 moment, in particular, is quite significant. Since the M_4 moment is governed by the acceleration of the morphing mass elements in the body frame, it is not surprising that the moment is greatest at the beginning and end of morphing. While the peak moment magnitude is large, the overall effect is somewhat muted by the fact that a positive moment spike at the onset of morphing is immediately followed by a negative spike at the conclusion of morphing. Thus, the overall behavior of the aircraft in the asymmetric turn is primarily determined by the aerodynamic forces and moments in the hold time between morphing events.

The qualitative behavior of the M_1 and M_4 moments is seen to be in agreement with expectations. As the left wing begins to flatten, it is rolling down in the body frame. This produces an instantaneous

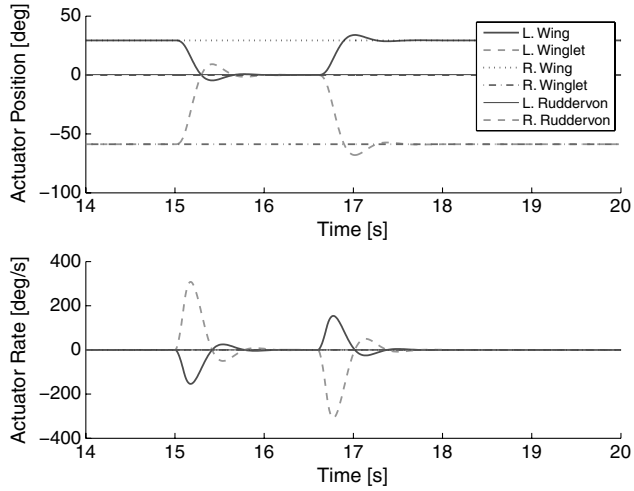

Fig. 7 The time dependence of the morphing angles during the asymmetric turn.

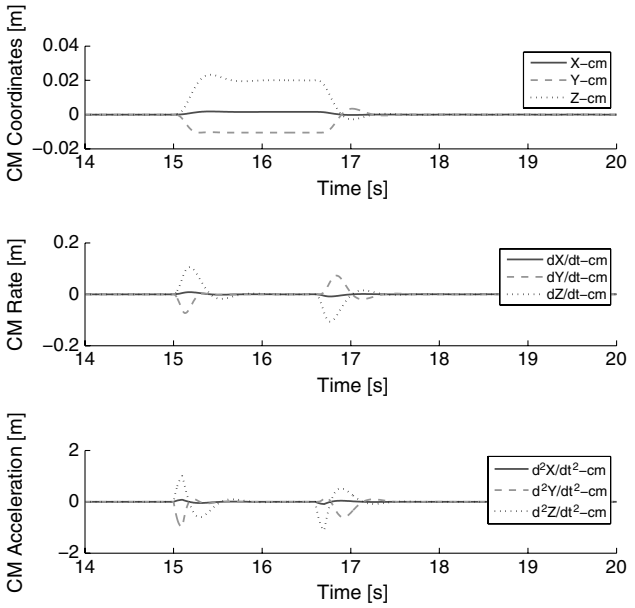

Fig. 8 The position, velocity, and acceleration of the CM in the body frame during the asymmetric turn.

moment opposing the motion so as to conserve angular momentum M_4. However, opposing the roll down of the left wing means rolling the body frame to the right, so that the initial M_4 rolling moment actually aids the turn. It will counter the turn as the morphing comes to an end, helping to stop the roll. The M_1 moment is preserving the angular momentum of a rotating body for which the inertia around the rotation axis is changing. Thus, it somewhat lags behind M_4, since the initial angular velocity is zero, and it is governed by the first (but not second) derivative of morphing. M_1 acts in a direction that initially opposes the turn, then it tries to continue it as the morphing ends. Thus, M_1 is, at all times, countering the control inputs. For this aircraft and maneuver, M_1 is quite small, and its influence is barely perceptible. These relative magnitudes of M_1 and M_4 are to be expected for a small UAV aircraft; the inertia tensor is small, but the accelerations of the morphing components are large. Morphing of a large aircraft would likely result in opposite behavior: a large inertia tensor and small accelerations.

The morphing forces, shown in Fig. 10, are also quite significant, primarily in the Y and Z directions. This is to be expected, since portions of the aircraft mass are accelerating within the body frame during morphing, resulting in the acceleration of the CM within the body frame. To preserve the instantaneous acceleration of the CM in the inertial frame, morphing forces are induced, as described by Eq. (18). Thus, it can be seen that as the left wing accelerates down and left in the body frame, the induced morphing forces are right and up (in the negative Z direction). The magnitudes are not negligible, being $\approx$10% of the aircraft weight. The X component of the morphing forces is much smaller, due to the minimal X motion of the CM within the body frame. Finally, the morphing force induced by the velocity of the CM [described by Eq. (19)] is considerably smaller than that induced by the acceleration of the CM. This is, in part, due to the fact that the angular velocity in Eq. (19) is small during the initial part of the turn, but it is more pronounced at the end of morphing.

It should also be noted that the magnitude of the morphing forces and moments is in large part determined by the morphing rates. The most significant moments and forces are governed by the first and second derivatives of the mass displacements, and it should therefore be expected that actuator frequencies play a crucial role in determining the impact of the morphing moments and forces. This is illustrated in Figs. 12 and 13.

The actuator frequencies of this aircraft are nominally set to $\omega = 20$ rad/s for modeling a fast actuator of a small UAV. The morphing (roll) moments for the fast actuator are shown in Fig. 12. If the actuator frequency is reduced to $\omega = 10$ rad/s, the simulation results (shown in Fig. 13) indicate a much smaller peak value of the morphing moments. The aerodynamic moment is only slightly changed, since it depends primarily on the instantaneous position and, to a lesser extent, on the velocity. In both cases, the commanded input was to transition from the symmetric to the asymmetric state in 0.1 s. The actual rate is thus determined by the actuator response times.

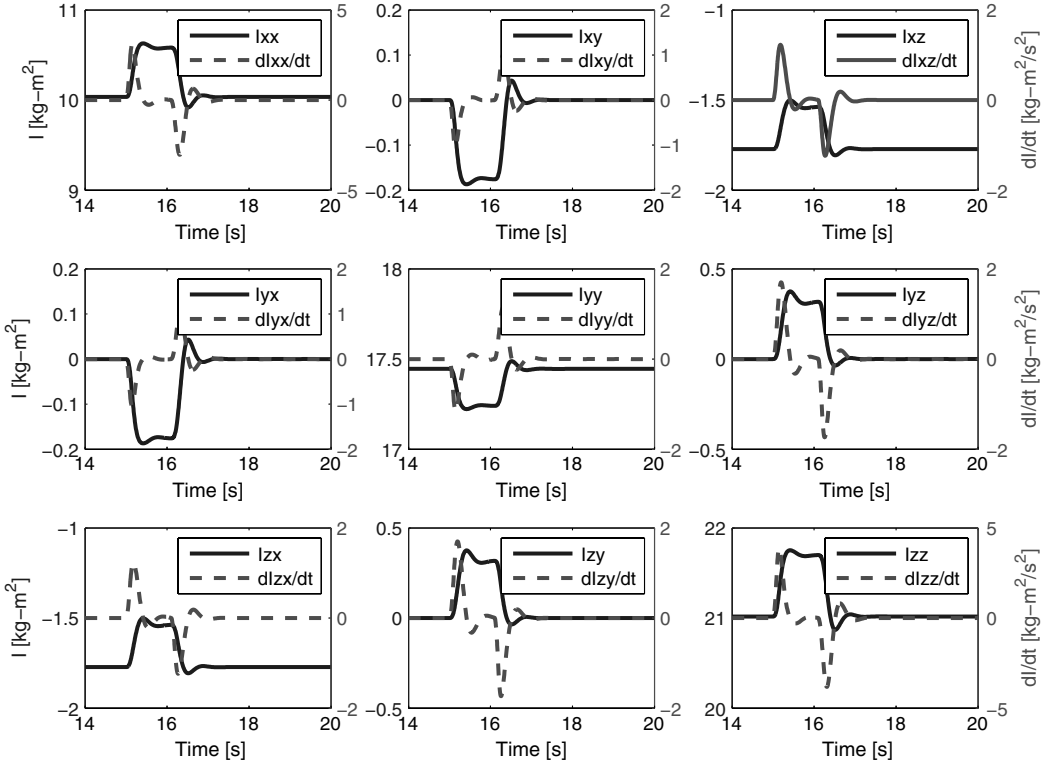

Fig. 9 The inertia tensor and its temporal derivative during the asymmetric turn.

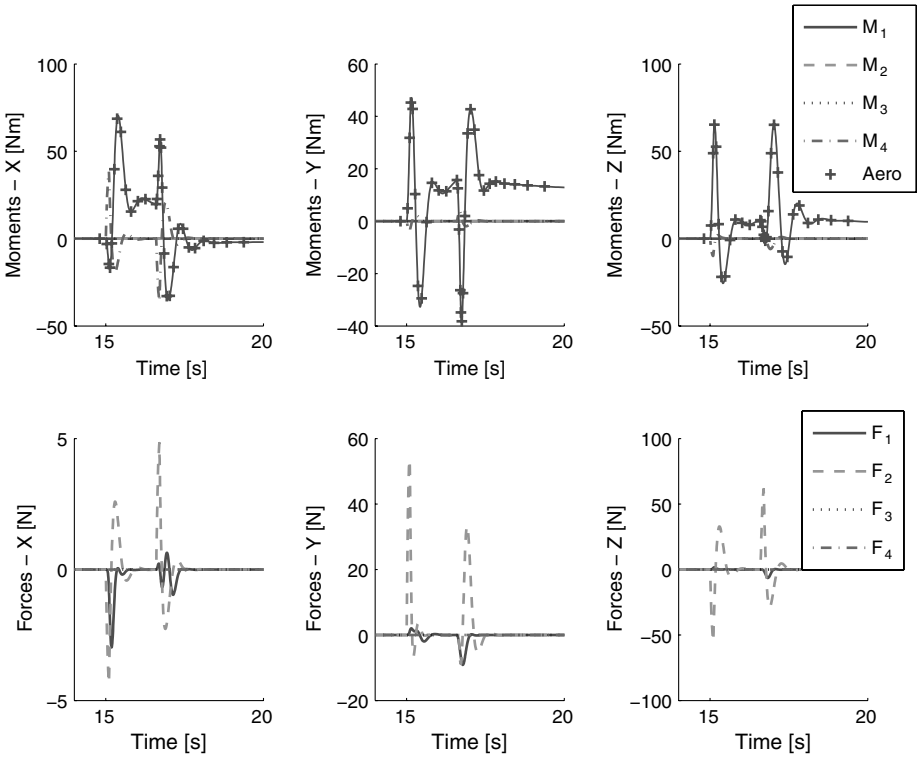

Fig. 10 The behavior of the morphing moments and forces during the asymmetric turn.

3. Numerics and Timing

As previously described, the ODE solution is based on an adaptive-time-step Runge–Kutta–Merson algorithm. The step size is controlled to keep the maximum relative truncation error at each time step below a user-defined threshold. If a larger error is estimated, the time point is rejected, the Δt is reduced, and the time point is attempted again.

The results for the asymmetric-turn simulation are shown in Fig. 14. The time step clearly had to be drastically reduced in order to resolve the morphing dynamics (driven by the within-body-frame

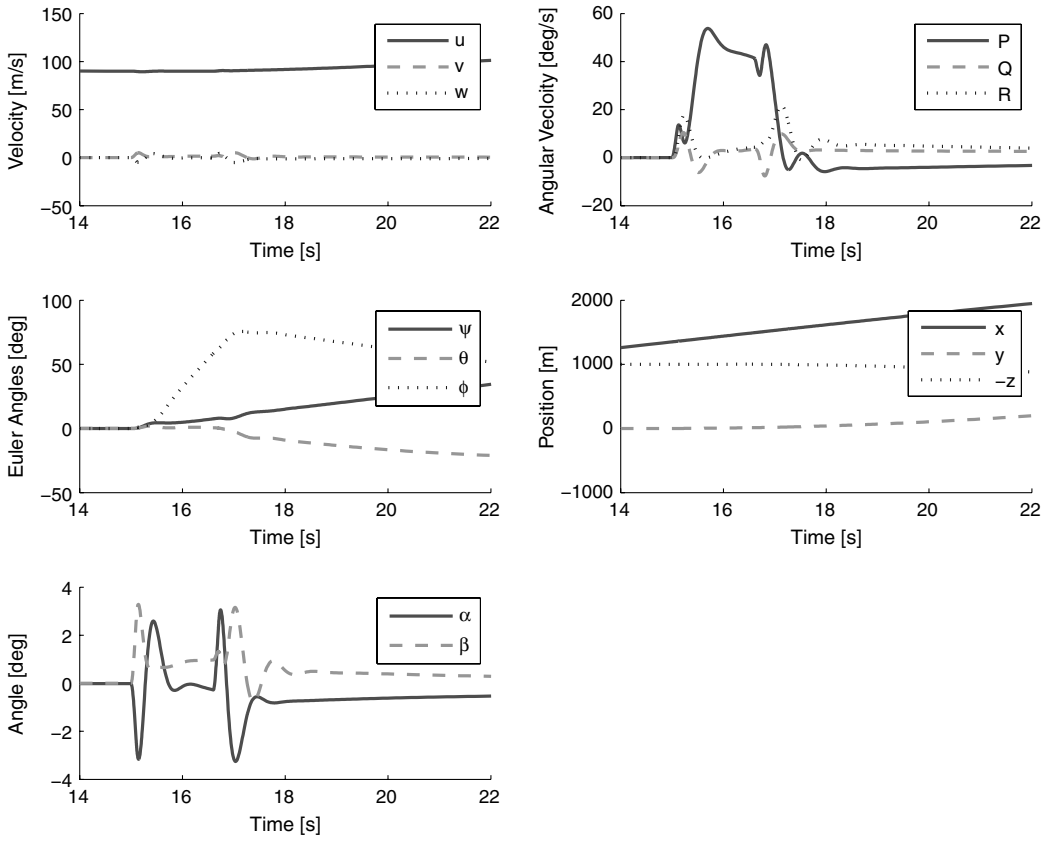

Fig. 11 Full state of the aircraft during the morphing portion of the trajectory.

acceleration), as evidenced by the small time steps used at the beginning and end of morphing. Adaptive time stepping is essential to performing this simulation in a reasonable time. Had a constant time step been used, the simulation time would have been nearly two orders of magnitude longer for the same level of truncation error.

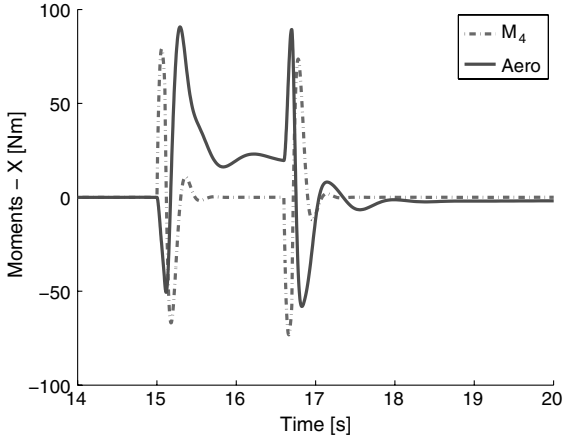

Fig. 12 Aerodynamic and M_4 morphing moments during the asymmetric turn, with actuator frequency $\omega = 20$ rad/s.

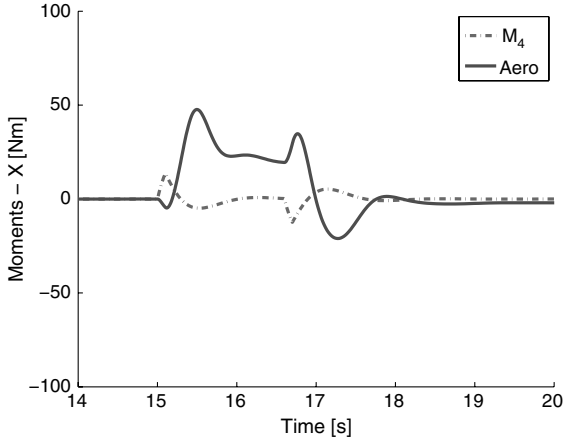

Fig. 13 Aerodynamic and M_4 morphing moments during the asymmetric turn, with actuator frequency $\omega = 5$ rad/s.

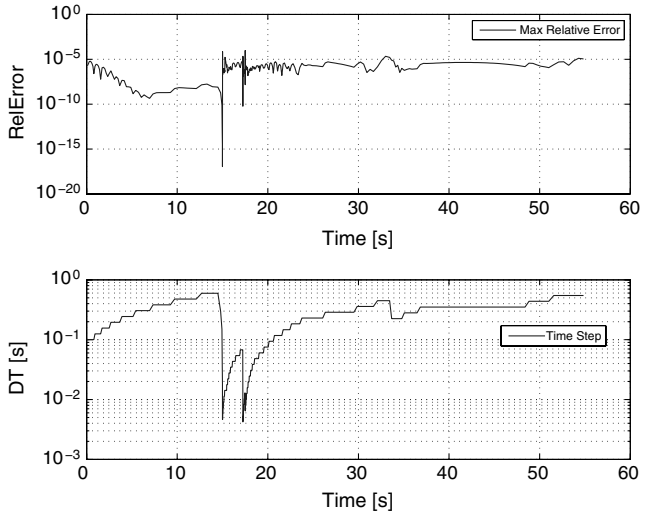

Fig. 14 The relative error and Δt at each time step (DT). Note the nearly two orders of dynamic range in the time steps used. Short time steps are required to resolve the dynamics during rapid morphing.

Table 2 Timing profile for asymmetric-turn simulation

Function	Type	Count	Time, s
VLM coefficient matrix	C++	2060	16.5
VLM linear solve	C++	2060	3.5
Aerodynamic forces	C++	2060	16.2
Morphing	C++	29238	3.4
Morphing moments	MATLAB	2060	37
Miscellaneous	MATLAB	——	20

The overall simulation takes ≈90 s of CPU time on a notebook computer for 60 s of simulated flight. The vortex-lattice calculation in compiled C++ (MATLAB MEX function) takes about 40 s, and the remainder of the time is taken up by various MATLAB functions: primarily the assembly of the RHS. The profile of the C++ code is summarized in Table 2 for a 2.5 GHz Intel Core 2 Duo MacBook Pro computer running with MATLAB 2008b. The C++ code was compiled using g++ 4.2.1 with the −O2 optimization option.

The third column indicates the number of calls to the particular module. The VLM coefficient matrix assembly and VLM linear

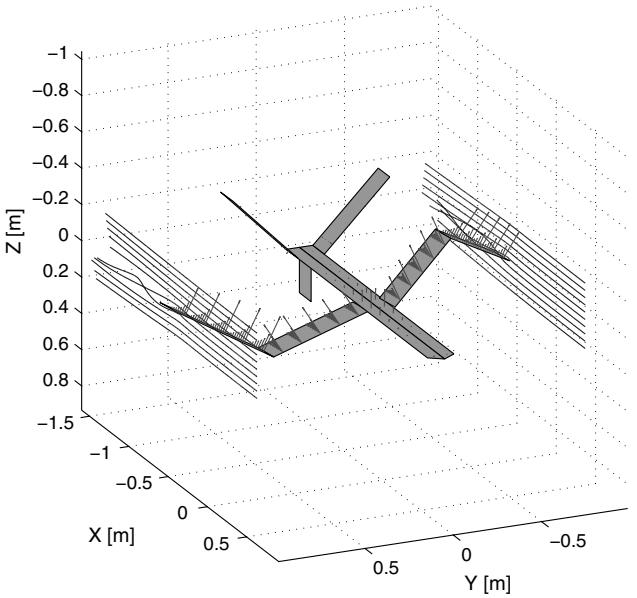

Fig. 15 The antisymmetric gull-wing configuration, with airflow streamlines and force vectors.

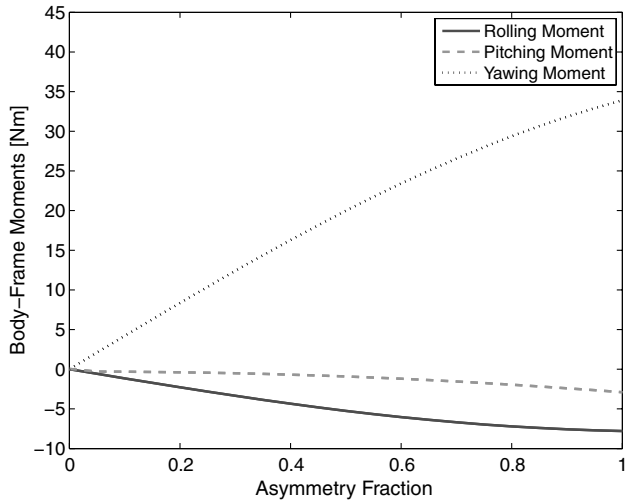

Fig. 16 The aerodynamic moments acting on the antisymmetric gull wing as a function of the asymmetry fraction, with 0° sideslip.

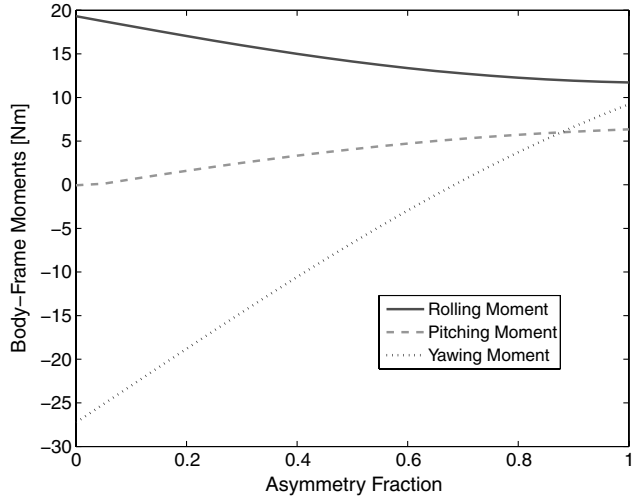

Fig. 17 Aerodynamic moments in the antisymmetric configuration with −1° sideslip.

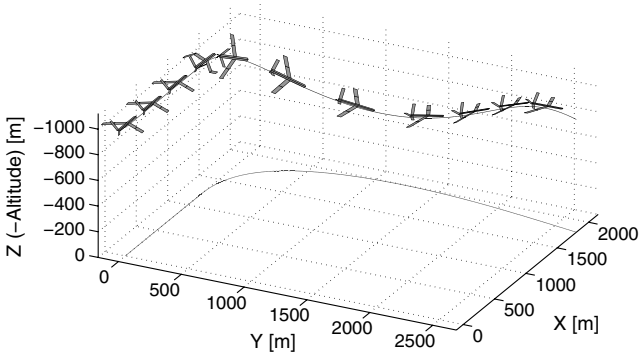

Fig. 18 Trajectory of the aircraft performing an antisymmetric turn.

solve modules are called approximately as many times as there are time steps in the simulation (somewhat more due to rejected time points), whereas the morphing module is invoked many more times due to the computation of virtual displacements needed to construct the time derivatives of the inertia tensor, the CM, and the positions of the planforms.

B. Antisymmetric Gull Wing

Another interesting possibility for inducing a turn using morphing is the antisymmetric wing morphing. The aircraft is assumed to start the maneuver in a flat-wing configuration, which is useful in a low-speed cruise. The right wing then morphs into a V shape, while the left morphs into an inverted V. This results in an antisymmetric wing arrangement, as shown in Fig. 15.

1. *Static Analysis*

Figure 15 illustrates the aerodynamic forces in the antisymmetric wing configuration. The resulting lift and moments are shown in Figs. 16 and 17. The aircraft experiences a significant yawing moment and a smaller rolling moment. The yawing moment arises due to a combination of the wing sweep, antisymmetric wing folding, and position of the CM. From Fig. 15, it can be seen that the forces acting on the outer wing surfaces have a positive Y component, whereas the inner panels have a negative Y component. Furthermore, the resultant of the inner panels is in front of the CM, while the resultant of the outer panels is behind it. Thus, a moment is generated around the CM. It can therefore be expected that the initial yaw moment during the turn will induce a negative sideslip angle. With negative sideslip, the positive yaw moment of the antisymmetric wing is competing with the negative yaw moment induced by the tail.

In addition to the yaw moment, a roll moment is induced. The roll moment arises due to the asymmetric placement of the CM with regard to the wings in the antisymmetric configuration. The CM is located at the midpoint of the wing planforms, slightly below the center of the fuselage planform. The resultants of the forces on each wing segment are approximately at the center of each segment. Because of this arrangement, the moment arm from the CM to the right outer wing section is slightly smaller than the moment arm to the left outer wing section. With the forces being equal, a slight negative roll moment results. However, the roll moment is actually negative only for very small slip angles. As the slip angle increases to $-1°$ or more (negative), the roll moment becomes positive. This is simply the swept-wing effect, with the lift of the leading wing increasing.

2. *Flight Simulation*

The flight trajectory induced by the antisymmetric turn is illustrated in Fig. 18. As in the case of the asymmetric turn, it should be expected that morphing moments play a significant role in the behavior of the aircraft. Indeed, it can be seen from Fig. 19 that morphing moments M_4 and M_1 are nonnegligible. M_4, in particular, is very significant, actually peaking above the aerodynamic moment. As expected, however, the morphing moments are present only during morphing. As in the asymmetric case, the morphing moments primarily impact the roll; the pitch and yaw morphing moments are almost negligible.

The behavior of the morphing roll moment can be understood intuitively as follows: as the wings fold from the flat configuration into the antisymmetric gull wing, they induce an intrabody-frame angular momentum. To conserve the instantaneous inertial-frame angular momentum, the body frame must roll in the opposite direction. This conservation of angular momentum manifests as the M_4 moment. Note that the initial M_4 moment is actually directed opposite to the subsequently induced aerodynamic moment. Thus, the body frame actually initially rolls away from the desired turn, as can be seen in Fig. 20. The roll angle initially dips to $\approx -20°$, before the aerodynamic moment takes over, and takes the aircraft into a positive roll. As in the case of the asymmetric roll, the morphing

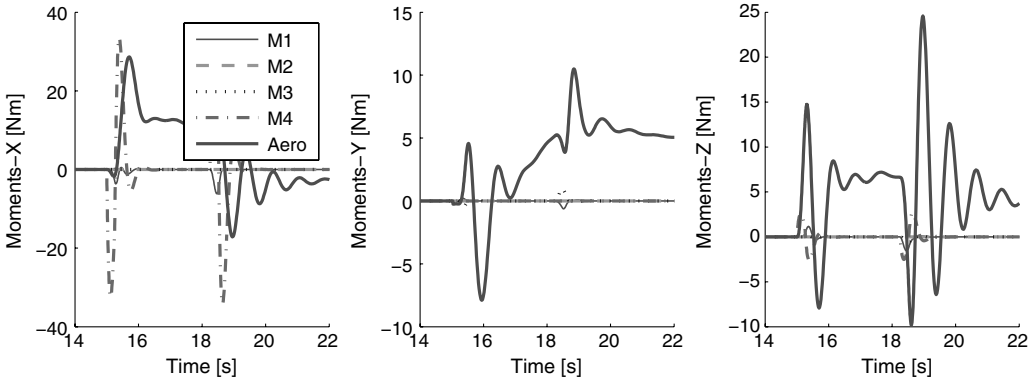

Fig. 19 Aerodynamic and morphing moments acting on the aircraft during the antisymmetric turn.

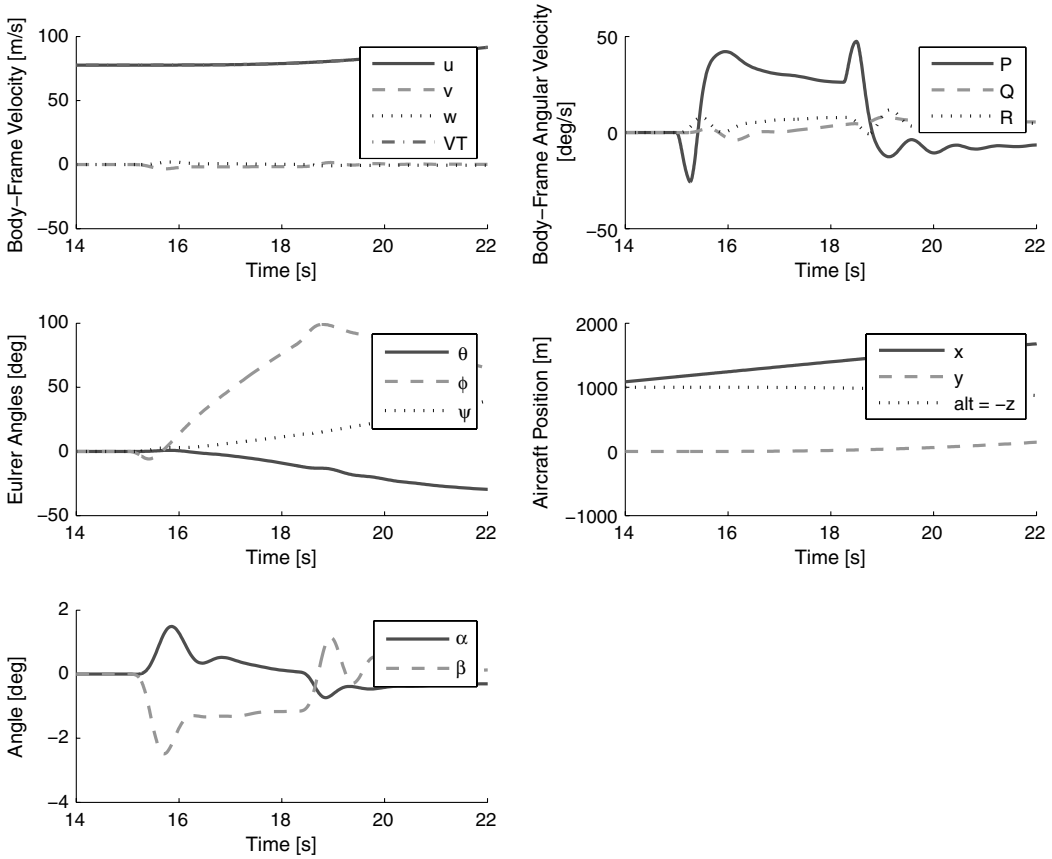

Fig. 20 State variables of the aircraft during the antisymmetric turn.

moments tend to act only briefly, so that it is generally the aerodynamic moments and forces that determine the overall behavior of the aircraft. Nevertheless, the initial influence of the morphing moments is quite significant in this case. Since the initial roll is actually away from the commanded direction, a feedback control system that monitors the body-frame roll angle may provide incorrect control inputs. Finally, the morphing forces during the antisymmetric turn are identically zero, due to antisymmetry; there is no intrabody-frame motion of the CM, and the expressions in Eqs. (18–20) vanish identically.

As can be expected from the behavior of the aerodynamic and morphing moments, the antisymmetric turning maneuver is somewhat complex. Because of the morphing moment M_4, the initial roll is indeed away from the desired turn direction, rolling to the left by more than 10°. As the wings approach the antisymmetric configuration and begin to slow down, the M_4 moment becomes aligned with the aerodynamic moment, sharply rolling the aircraft to the right. This results in a $\approx$90° bank to the right.

At the same time, the aerodynamic yaw moment is turning the nose of the aircraft to the right, inducing a negative sideslip. Some oscillation in the sideslip ensues, resulting from the balance of the positive wing yaw moment and negative tail yaw. Finally, as the morphing maneuver ends and the wings are restored to the flat configuration, the aircraft returns to nearly level flight (although still turning gently), having completed a $\approx$90° turn.

V. Conclusions

An efficient simulation methodology specifically tailored for morphing aircraft has been developed. The methodology handles both the aerodynamic and inertial effects of wing morphing, or other active structural modifications. The aerodynamics are handled by an efficient run-time VLM capable of properly handling the morphing aircraft structure. The EOMs of the aircraft have been modified to account for the time dependence of the aircraft configuration by including morphing moments and forces. The methodology is applicable to a wide range of aircraft structures, with arbitrary combinations of planforms and joints possible. The computational requirements are significantly reduced relative to a multibody dynamics scheme. The key limitation relative to a multibody dynamics code is the approximate treatment of the actuator and structural dynamics. The simulation methodology has been applied to various wing morphing states, and the behavior of the aircraft have been analyzed under both static (wind tunnel) and dynamic (nonlinear flight simulation of a morphing-induced turn) conditions.

The principal result of the simulation study is that significant morphing forces and moments can act on the aircraft if the morphing displacements are large in amplitude or if the morphing is rapid (even if small in amplitude). Under those conditions, modeling the aircraft using rigid-body dynamics with a time-varying inertia tensor proves to be insufficient. The dominant morphing forces and moments are proportional to the intrabody-frame accelerations of wing mass components, and therefore tend to primarily influence the dynamics at the onset and end of a morphing maneuver. Furthermore, the morphing forces and moments can oppose the desired aerodynamic effects of morphing, at least in the initial and final stages of morphing. This effect must be taken into account when designing control systems for morphing aircraft.

References

[1] Weisshaar, T., "Morphing Aircraft Technology: New Shapes for Aircraft Design," NATO Rept. RTO-MP-AVT-141, 2006, http://www.dtic.mil/cgi-bin/GetTRDoc?Location=U2\&doc= GetTRDoc.pdf\&AD=ADA479821 [retrieved 1 July 2009].

[2] Davidson, J., Chwalowski, P., and Lazos, B., "Flight Dynamic Simulation Assessment of a Morphable Hyper-Elliptic Cambered Span Winged Configuration," AIAA Atmospheric Flight Mechanics Conference, AIAA Paper 2003-5401, Aug. 2003.

[3] Bowman, J., Sanders, B., and Weisshaar, T., "Evaluating the Impact of Morphing Technologies on Aircraft Performance," AIAA/ASME/ASCE/AHS/ASC Structures, Structural Dynamics, and Materials Conference, AIAA Paper 2002-1631, April 2002.

[4] Manzo, J., and Garcia, E., "Evolutionary Flight and Enabling Smart Actuator Devices," *Active and Passive Smart Structures and Integrated Systems 2007*, SPIE Paper 6525, Bellingham, WA, March 2007.
[5] Grant, D., Chakravarthy, A., and Lind, R., "Modal Interpretation of Time-Varying Eigenvectors of Morphing Aircraft," AIAA Atmospheric Flight Mechanics Conference, AIAA Paper 2009-5848, Aug. 2009.
[6] Grant, D., and Lind, R., "Effects of Time-Varying Inertias on Flight Dynamics of an Asymmetric Variable-Sweep Morphing Aircraft," AIAA Atmospheric Flight Mechanics Conference and Exhibit, AIAA Paper 2007-6487, Aug. 2007.
[7] Grant, D., Abdulrahim, M., and Lind, R., "Flight Dynamics of a Morphing Aircraft Utilizing Independent Multiple-Joint Wing Sweep," AIAA Atmospheric Flight Mechanics Conference and Exhibit, AIAA Paper 2006-6505, Aug. 2006.
[8] Chakravarthy, A., Grant, D., and Lind, R., "Time-Varying Dynamics of a Micro Air Vehicle with Variable-Sweep Morphing," AIAA Guidance, Navigation, and Control Conference, AIAA Paper 2009-6304, Aug. 2009.
[9] Yue, T., and Wang, L., "Multibody Dynamic Modeling and Simulation of a Tailless Folding Wing Morphing Aircraft," AIAA Atmospheric Flight Mechanics Conference, AIAA Paper 2009-6155, Aug. 2009.
[10] Valasek, J., Lampton, A., and Marwaha, M., "Morphing Unmanned Air Vehicle Intelligent Shape and Flight Control," AIAA Infotech at Aerospace Conference, AIAA Paper 2009-1827, April 2009.
[11] Scarlet, J. N., Canfield, R. A., and Sanders, B., "Multibody Dynamic Aeroelastic Simulation of a Folding Wing Aircraft," 47th AIAA/ASME/ASCE/AHS/ASC Structures, Structural Dynamics, and Materials Conference, AIAA Paper 2006-2135, May 2006.
[12] Blundell, M., and Harty, D., *Multibody Systems Approach to Vehicle Dynamics*, Elsevier, Burlington, MA, 2004.
[13] Shabana, A. A., *Dynamics of Multibody Systems*, 3rd ed., Cambridge Univ. Press, New York, 2005.
[14] Sequeira, C. J., Willis, D., and Peraire, J., "Comparing Aerodynamic Models for Numerical Simulation of Dynamics and Control of Aircraft," AIAA Aerospace Sciences Meeting, AIAA Paper 2005-0854, May 2005.
[15] Melin, T., "Tornado: A Vortex Lattice MATLAB Implementation for Linear Aerodynamic Wing Applications," M.S. Thesis, Royal Inst. of Technology, Stockholm, 2000.
[16] Selitrnnik, E., and Karpel, M., "Generalized Approach to Aeroelastic CFD Time Simulations of Morphing Flight Vehicles," 50th AIAA/ASME/ASCE/AHS/ASC Structures, Structural Dynamics, and Materials Conference, AIAA Paper 2009-2323, May 2009.
[17] Wittenburg, J., *Dynamics of Multibody Systems*, 2nd ed., Springer-Verlag, New York, 2002.
[18] Katz, J., and Plotkin, A., *Low-Speed Aerodynamics*, 2nd ed., Cambridge Univ. Press, New York, 2001.
[19] Ousterhout, J. K., *Tcl and the Tk Toolkit*, Addison-Wesley Professional Computing Series, Addison Wesley Longman, Reading, MA 1994.
[20] Bertin, J., and Smith, M., *Aerodynamics for Engineers*, Prentice–Hall, Englewood Cliffs, NJ, 1979.
[21] Goldstein, H., *Classical Mechanics*, Addison Wesley, New York, 2001.